Modeling and System-Level Performance Evaluation of Sub-Band Full Duplexing for 5G-Advanced

Karchegani, Masoumeh Mokhtari; Pocovi, Guillermo; Maldonado, Roberto; Pedersen, Klaus Ingemann

Published in:
IEEE Access

DOI (link to publication from Publisher):
10.1109/ACCESS.2023.3295121

Publication date:
2023

Document Version
Accepted author manuscript, peer reviewed version

Modeling and System-Level Performance Evaluation of Sub-Band Full Duplexing for 5G-Advanced

MASOUMEH MOKHTARI[2] (Student Member, IEEE), GUILLERMO POCOVI[1], ROBERTO MALDONADO[1] and KLAUS I. PEDERSEN[1,2] (Senior Member, IEEE)
[1]Nokia, 9220 Aalborg, Denmark
[2]Department of Electronic Systems, Aalborg University, 9100 Aalborg, Denmark
Corresponding author: Masoumeh Mokhtari (e-mail: mmka@es.aau.dk).

ABSTRACT This article presents sub-band full duplex (SBFD) as a duplexing scheme to improve the uplink (UL) throughput in 5G–Advanced networks, as an alternative to traditional time-division duplexing (TDD). SBFD provides opportunities to transmit and receive simultaneously on non-overlapping frequency resources. To accomplish this, SBFD time slots include both UL and downlink (DL) transmission. This leads to UL transmission being more expanded in the time domain rather than the frequency domain, which allows to increase the amount of UL transmission opportunities, as compared to TDD where the majority of time slots are used for DL. Concurrent UL and DL transmission create different types of interference, which makes cancellation approaches essential for appropriate performance. The SBFD interference types, including self-interference as the main challenge of SBFD deployment, are outlined and corresponding analytical models are proposed to provide a realistic evaluation of SBFD performance. System-level simulations with different load conditions in a high-power urban macro environment are used to evaluate the SBFD performance in comparison with TDD as the baseline. The results indicate a four times increase in the UL throughput for cell-edge users as well as 32% and 6% increase in average UL throughput, at low and medium loads, respectively. Furthermore, simulation results determine that at least 149 dB of self-interference mitigation is required for acceptable performance in SBFD. Results also show that SBFD benefits are limited by inter-site gNB-to-gNB interference.

INDEX TERMS 5G-Advanced, uplink coverage, self-interference, interference modeling, system-level performance.

I. INTRODUCTION

The standardization of the fifth generation of cellular networks (5G) was started by the Third Generation Partnership Project (3GPP) with the first 5G specifications, appearing in Release 15 (Rel-15). Rel-18 marks the start of the 5G-Advanced era, where 5G is taken to its fullest capabilities by introducing numerous new functionalities and enhancements to existing schemes that were introduced in earlier 5G releases [1]. The 5G New Radio (NR) standard, and earlier mobile networks standards, were mainly developed to accommodate the ever-increasing downlink (DL) traffic demands, although several uplink (UL) enhancements, were naturally also included. Recently, uplink (UL) traffic demands have started to increase significantly [2] due to the emergence of new UL-heavy services and applications, e.g., extended reality (XR) applications with live video feeds from devices. Consequently, the 5G-Advanced standard aims to further enhance the overall uplink performance. The majority of the spectrum available for NR deployments is unpaired with the default duplexing scheme being time-division duplexing (TDD), where 5G base stations (gNBs) and user equipment (UE) transmit using the same frequencies at different times, as illustrated in Fig. 1. TDD has some advantages over frequency-division duplexing (FDD), such as lower complexity on devices and flexibility of distributing the resources between UL and downlink (DL) in time-domain [3]. The 5G NR standard is designed to support highly flexible configurations for TDD deployments and allows deployments to adopt dynamic TDD, in which the link direction per slot dynamically changes with the instantaneous traffic demands. Dynamic TDD has been extensively studied in the open literature, with examples in [4]–[6], showing attractive benefits for single-operator cases if handling the TDD cross-link interference (CLI) with care. However, in realistic multi-

operator cases, where operators are assigned neighboring carrier frequencies within the same unpaired carrier band, it has been found that fulfilling the inter-operator co-existence requirements in most macro deployment cases prevent the use of dynamic TDD deployment [7], [8]. Instead, fully synchronized static DL-heavy radio frame configurations are adopted by the operators to accommodate large volumes of DL data, in line with regulatory requirements. By doing this, no inter-operator (i.e., inter-frequency) CLI occur, and also intra-carrier co-channel CLI is avoided. The disadvantage of applying such static DL-heavy TDD radio frames configurations is reduced UL coverage due to the sparse availability of only one time slot out of every five slots for UL transmission [9], [10].

New duplexing solutions to enhance the UL performance are therefore gaining more interest. In the past, full duplex schemes were studied as a solution to boost UL transmission opportunities by allowing UL and DL transmission at the same overlapping radio resources. Traditional full duplex (FD) refers to simultaneous transmission and reception at the gNB on overlapping frequency resources, which has the potential to double the spectral efficiency, and reduce packet latency [11], [12], [13]. Nevertheless, FD introduces new types of interference that are not present in today's TDD or FDD networks, including gNB self-interference as well as UE-to-UE and gNB-to-gNB CLI [14]. Consequently, advanced interference mitigation techniques are required to suppress interference to a reasonable level [12], [15]. In [16], the authors show that FD operation outperforms TDD in terms of throughput and latency, under the assumption of ideal self-interference and CLI mitigation, while in case of significant inter-cell interference, TDD may provide better performance. Similarly, [17], [18] show that the theoretical 100 % FD gain is achievable only under specific assumptions, including ideal self-interference mitigation, isolated cell, and full buffer traffic model, while the lower gain is generally achieved under realistic multi-cell and dynamic traffic scenarios [18]. Consequently, in the short term, FD is currently not yet seen as practical for multi-cell cellular networks with real-world traffic patterns, as also concluded in [19], although pursuing FD for future systems such as 6G is still an active research area. For further insight on FD, we refer to the two comprehensive textbooks in [14] and [13].

More recently, sub-band full duplex (SBFD) has emerged as a new promising approach that allows simultaneous UL and DL transmission on non-overlapping frequency resources in the same unpaired TDD carrier [3], [20] as pictured in Fig. 2. Contrary to traditional FD, SBFD does not intend to increase the total (UL + DL) resource availability, but instead, it allows more frequent availability of UL resources as compared to traditional TDD, as well as slots with simultaneous UL and DL resources. Despite SBFD appearing similar to FDD, there are several differences. Firstly, FDD employs separate frequency bands for UL and DL communication with a large guard band in-between to prevent any potential cross-link interference. In contrast, SBFD utilizes a single

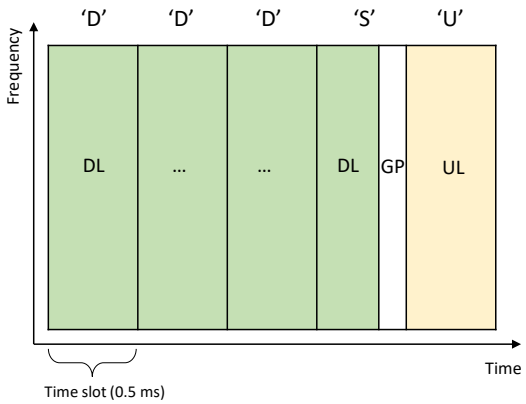

FIGURE 1. Considered TDD frame structure.

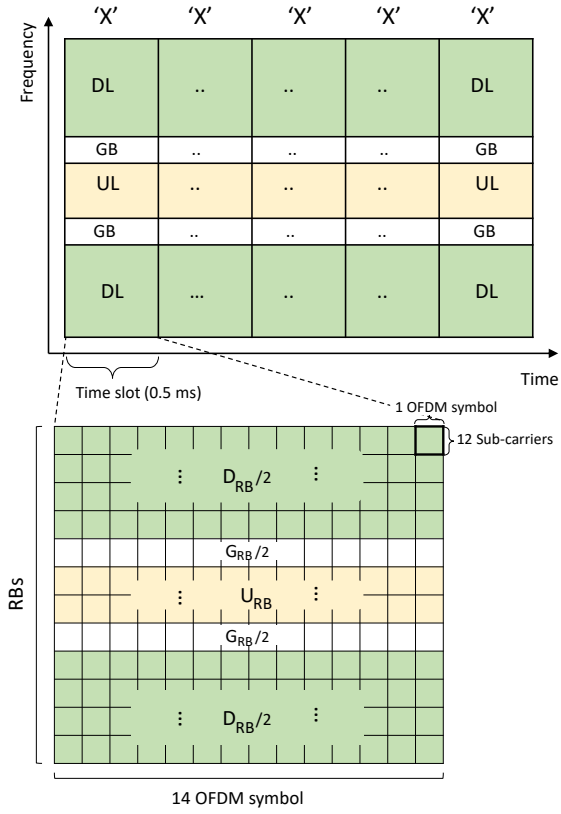

FIGURE 2. Proposed SBFD frame structure.

frequency band for both UL and DL (as used today for TDD) which may result in interference primarily due to power leakage from DL to the UL transmission and vice versa. Moreover, in FDD, the uplink and downlink frequency bands, have generally the same size, while they can be asymmetrical in SBFD as illustrated in Fig.2.

Adopting SBFD in 5G-Advanced is expected to reduce the latency and improve UL coverage, especially for cell-edge UEs who can only transmit over a limited set of frequency resources at a time. SBFD comes with the benefit of less strict requirements on the self-interference mitigation at the

gNB, due to no overlap between DL and UL resources. However, the CLI is still present due to different transmitter and receiver imperfections. These imperfections cause leakage of the power transmitted on the allocated resources into adjacent frequencies, which creates interference and damages the reception over the adjacent resources. SBFD was presented and studied in [3] (under the name of cross-division duplex, XDD), where authors show that SBFD is able to extend the maximum radio distance by 54 % compared to TDD, which is equivalent to 2.37 times larger coverage area. The focus of [3] is on self-interference suppression techniques and shows that a combination of antenna isolation (i.e. separate transmit-receive antennas at gNB) and digital self-interference cancellation (SIC) is required to achieve an acceptable performance. Recently, authors in [20] studied SBFD performance in dense urban and indoor scenarios, and proposed a framework for interference coordination to manage gNB-to-gNB interference. Their simulation results show a notable gain of SBFD in UL throughput and latency, as well as, a minor performance reduction in DL. This study indicates that a lower DL load increases the UL throughput due to the lower self-interference and gNB-to-gNB CLI.

This study presents a comprehensive analysis of the performance of SBFD in a realistic Urban Macro (UMa) environment, with multiple users and time-varying interference and traffic. As SBFD is a relatively new concept, this paper first discusses and proposes models for gNB self-interference, gNB-to-gNB, and UE-to-UE cross-link interference. New interference models are derived since existing models for FD in the literature cannot be applied as the interference originates from leakage emissions due to transmitter/receiver imperfections and non-linearities. Based on these models, the SBFD performance is studied with a focus on the impact of the different types of interference for different loads of traffic and self-interference mitigation capabilities at the gNB. The paper is aligned with the currently ongoing 3GPP Rel-18 NR study item on duplexing evolution, as part of 5G-Advanced standardization, which targets to assess the feasibility and performance of SBFD for different network deployments and frequency ranges [21]. The main contributions of this work are listed in the following:

- We propose precise analytical models of the different interference types in SBFD scenarios, including self-interference, gNB-to-gNB cross-link interference, and UE-to-UE cross-link interference, which are essential to accurately understand the performance of SBFD operation.
- We study the contribution of each individual interference component on the SBFD performance for different levels of self-interference mitigation at the gNB.
- The SBFD performance under different offered load conditions is studied to discover its benefits as well as its weaknesses compared to baseline TDD.
- Based on the obtained results, the recommendation for the required level of self-interference mitigation is provided based on trade-offs between gNB complexity and performance gains.

The complexity of our system model prevents a purely analytical evaluation without omitting many important practical aspects. For this reason, a hybrid methodology is adopted in this study, where models are first derived in an analytical manner, and then implemented in a system-level simulator, which is used as the primary tool to quantify the overall system performance. The simulator follows the 5G NR evaluation methodology agreed upon in the 3GPP, including explicit and detailed modeling of the majority of radio resource management (RRM) functionalities, which are known to have a major impact on the radio performance. When conducting such simulations, good practices are applied to ensure trustworthy results. This includes realistic simulation assumptions as well as collecting enough samples to provide sustainable statistics, using a Monte Carlo methodology with multiple users drops.

The rest of the paper is organized as follows. Section II describes the considered network and UE deployment assumptions, including SBFD frame configuration and adopted traffic model. This section also details the examined key performance indicators (KPIs), antenna configuration aspects, and RRM considerations. Section III outlines the different interference types in SBFD and presents the proposed interference modeling. The evaluation methodology and simulation assumptions are presented in Section IV. The performance results are shown in Section V, followed by concluding remarks in Section VI. Additionally, a list of abbreviations is provided at the end of the manuscript.

II. PROPOSED SYSTEM MODEL

A. SETTING THE SCENE

An UMa cellular network is considered with C cells placed in a sectorized manner on a hexagonal grid; 7 sites with three cells each (covering a 120° sector) for a single operator deployment, and 500 m inter-site distance (ISD). Note that, the terms "cell", "base station" and "gNB" are used interchangeably in this article. U UEs are uniformly distributed in outdoor and indoor locations, across the entire network area. Each gNB is equipped with N antennas, while UEs are equipped with M antennas. Each user generates both UL and DL traffic and operates in a half-duplex manner, i.e., it transmits and receives at different times. UL and DL signals from/towards different users are dynamically multiplexed on a time-frequency grid of resources, using orthogonal frequency division multiple access (OFDMA). The radio resources are assigned with a resolution of one resource block (RB), composed of 14 OFDM symbols in the time domain and 12 sub-carriers in the frequency domain, as shown in Fig. 2. A 5G NR-compliant physical layer design is assumed with 30 kHz subcarrier spacing (SCS), resulting in a slot duration of 0.5 ms and RB bandwidth of 360 kHz [22]. The assumed carrier bandwidth is 100 MHz corresponding to $P_{\mathrm{RB}} = 273$ RBs after accounting for the mandatory inter-operator guard-bands.

For the baseline TDD cases as pictured in Fig. 1, each slot is used for either UL or DL transmissions (denoted as 'U' or 'D' slot, respectively), while SBFD slots are used for simultaneous UL and DL, denoted as 'X' slot (Fig. 2). In each SBFD slot, U_{RB} and D_{RB} RBs are configured for UL and DL transmission, respectively. The group of contiguous RBs for a given link direction is also known as sub-band. The SBFD slot configuration is assumed to have 2 DL and 1 UL sub-bands. A guard band of $G_{\text{RB}}/2$ RBs is introduced in between two sub-bands of opposite link directions to improve the isolation between transmission and reception. In line with the ongoing 3GPP discussions [23], the UL sub-band is placed in the middle of the carrier bandwidth following the sequence $(D_{\text{RB}}/2, G_{\text{RB}}/2, U_{\text{RB}}, G_{\text{RB}}/2, D_{\text{RB}}/2)$, with $P_{\text{RB}} = U_{\text{RB}} + D_{\text{RB}} + G_{\text{RB}}$. In the time-domain, without loss of generality, a SBFD frame structure 'XXXXX' is assumed for all the gNBs, i.e., SBFD operation with fixed $U_{\text{RB}}, D_{\text{RB}}, G_{\text{RB}}$ split is assumed for all the time slots, while options with time-varying UL-DL RB split are also possible e.g., 'XXXXU', which has been studied in [20].

B. TRAFFIC MODELING AND KPIS

The generated traffic follows the file transfer protocol model 3 (FTP3), in which fixed packets of B bits are generated for each UE in both DL and UL directions. The packet arrival per UE follows a Poisson Arrival Process with different packet arrivals [packet/s] of λ^{dl} and λ^{ul} for DL and UL direction, respectively. The generated traffic load per UE in the DL direction is: $L^{dl} = \lambda^{dl} \times B$ [bps], and, in the same way, the traffic load in the UL direction is: $L^{ul} = \lambda^{ul} \times B$ [bps]. Consequently, DL offered load per cell can be calculated as: $L^{dl}_{c_i} = \lambda^{dl} \times B \times U_{c_i}$[bps] where U_{c_i} refer to the number of users associated to cell c_i, and, in the same manner, UL offered load per cell is: $L^{ul}_{c_i} = \lambda^{ul} \times B \times U_{c_i}$[bps]. Simulations are run for different levels of offered load to reflect different network load conditions.

The main examined KPI is the experienced user throughput per link direction. For each generated packet of index j, the throughput per packet is calculated as the total amount of bits B in the packet divided by the time T_j [s] it took to successfully transmit the packet:

$$th_{pkt_j} = \frac{B}{T_j} \ . \tag{1}$$

Based on this, the average UE perceived throughput, denoted as Th_{ue} [bps], is calculated as the average of the throughput of the packets transmitted or received by each UE i, i.e.:

$$Th_{ue_i} = \frac{1}{N^i_{pkt}} \sum_{j=1}^{N^i_{pkt}} th_{pkt_{j,i}} \ , \tag{2}$$

where N^i_{pkt} corresponds to the number of received packets (in either UL or DL direction) for the i-th user during the simulation time.

C. ANTENNA CONFIGURATION

For the considered SBFD deployment, gNB's antenna design is assumed to employ separate antenna elements for transmission and reception to provide spatial isolation (more details in Sec. III-A1), whereas in TDD all antenna elements are used to transmit and receive. Consequently, doubling the number of antenna elements is required for SBFD to obtain the same antenna gain as in TDD. In this study, $N_g \times M_g \times P_g$ antenna elements, (N_g columns, M_g rows, and P_g polarization dimension) are considered for TDD baseline whereas in SBFD $N_g \times M_g \times P_g$ antenna elements for reception and a same number of antenna elements for transmission are assumed. Therefore, the total number of antenna elements will be $N_g \times 2M_g \times P_g$ for SBFD deployment as illustrated in Fig. 3.

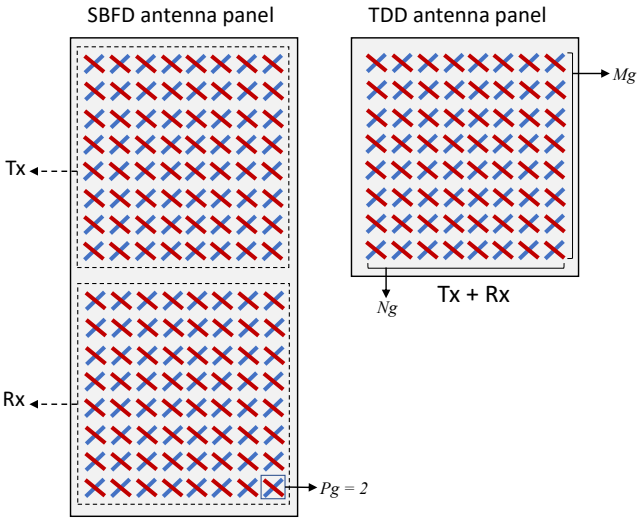

FIGURE 3. Considered antenna configuration for TDD and SBFD.

Digital single-user multiple-input multiple-output (SU-MIMO) with the dual-stream transmission for DL and single-stream for UL direction are assumed, using Type-I precoders [22]. At the receiver-side, a linear minimum mean square error interference rejection combining (MMSE-IRC) receiver is assumed [24].

D. RADIO RESOURCE MANAGEMENT

Dynamic link adaptation is assumed for all users by adjusting the modulation and coding scheme (MCS) per transmission. For each DL transmission, the MCS index is selected based on the channel quality indicator (CQI) reported by the UEs, which indicates the largest supported data rate without exceeding a block error rate (BLER) of P_{target}. The default setting for the BLER target is $P_{target} = 0.1$. The CQI report is determined by the UE by measuring the DL signal-to-interference and noise ratio (SINR) which is mapped to a CQI index by having knowledge of the BLER versus SINR for each supported MCS. In addition, due to the UE SINR

estimation imperfections and CQI reporting delays (during which the SINR conditions may change), the well-known outer loop link adaptation (OLLA) algorithm is assumed, where the received CQI values are offset by a certain factor O (OLLA offset). This factor O is increased in case of receiving NACK and decreased if receiving an ACK [25].

The DL resource allocation procedure is based on transmission time intervals (TTIs). On every TTI, each cell c_i independently allocates resources to its associated users (U_{c_i}). Each RB p is assigned to the user ue_i^* that maximizes the proportional fair (PF) metric,

$$ue_{i,p}^* = \arg\max_{ue_i} \left\{ \frac{r_{ue_i,p}[t]}{Th_{ue_i}[t]} \right\}, \quad (3)$$

where t is the discrete time index for the scheduling interval, $r_{ue_i,p}$ is an estimate of the instantaneous supported data rate of user ue_i in the p^{th} RB, and Th_{ue_i} is the average delivered user throughput in the past interval. The value of $r_{ue_i,p}$ is estimated based on the periodical frequency-selective CQI report sent by each UE, whereas $Th_{ue_i}[t]$ is calculated recursively using a moving average filter and it is updated only for the users with buffered data [25].

For UL, the gNB uses the sounding reference signal (SRS) transmitted by each of the active UEs to estimate the channel state information (CSI). This CSI is used by the link adaptation unit to select the appropriate MCS. An OLLA algorithm is adopted to compensate for the link adaptation delay and SINR measurement errors. The OLLA offset adjustments occur based on ACK/NACK from first transmissions [26]. Asynchronous hybrid automatic repeat request (HARQ) with chase combining for both link directions is assumed. The UE transmit power $P_{\text{Tx}}^{\text{UE}}$ determines the reception quality from the UE at the serving cell. The UE transmit power is subjected to open-loop power control that is controlled by two parameters, namely the path-loss compensation factor, α, and the target power spectral density per RB p_0. Consequently, $P_{\text{Tx}}^{\text{UE}}$ [dBm] formulates as:

$$P_{\text{Tx}}^{\text{UE}} = \min\{P_{max}, p_0 + 10\log_{10}(N_{\text{UL-RB}}) + \alpha \cdot PL\}, \quad (4)$$

where P_{max} is the maximum UE transmit power, $N_{\text{UL-RB}}$ indicates the number of allocated UL RBs, and PL refers to the measured path-loss by the UE [27], [28]. The UL resource allocation follows the adaptive transmission bandwidth-based packet scheduling, presented in [29]. On every TTI, the channel quality metrics of the active UEs are calculated for each RB according to their transmitted SRS. The RB allocation starts with the highest UE quality metric value and the bandwidth expands until the UE receives the required RB allocation to transmit the buffered data, the UE transmit power $P_{\text{Tx}}^{\text{UE}}$ reaches its maximum, or all the available resources have been allocated.

III. INTERFERENCE MODELING

The following six types of co-channel interference are present in SBFD as pictured in Fig. 4:

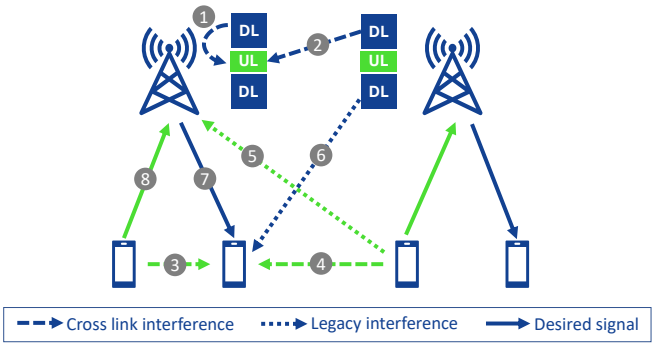

FIGURE 4. Different types of co-channel interference for SBFD.

1) **gNB self-interference (SI):** SI refers to the receive antennas of the gNB capturing the interfering signals from its own transmit antennas.
2) **gNB-to-gNB co-channel inter-subband CLI:** Interference at a gNB receiver from another gNB transmitting on non-overlapping frequency resources.
3) **Intra-cell UE-to-UE co-channel inter-subband CLI:** Interference at a UE receiver from another UE connected to the same cell and transmitting on non-overlapping frequency resources.
4) **Inter-cell UE-to-UE co-channel inter-subband CLI:** Interference at a UE receiver from another UE connected to a neighbor cell of the serving cell and transmitting on non-overlapping frequency resources.
5) **Inter-cell UE-to-gNB UL co-channel legacy interference:** The interference of UL transmission of one UE to the UL reception of other cells gNBs.
6) **Inter-cell gNB-to-UE DL co-channel legacy interference:** The interference of DL transmission of gNB to the DL reception of other cells UEs.

A. SIGNAL MODEL

Let us denote $\mathcal{C} = \{1, ..., C\}$ as the set of cells, and K_{dl} and K_{ul} as the set of UEs with active DL and UL transmissions during a given slot t, respectively. In the slot t, the received DL signal $\mathbf{y}_{k,c_k}^{dl\,(m,t)}$ for UE k ($k \in K_{dl}$) with serving cell c_k ($c_k \in \mathcal{C}$) over a specific resource block (m), is expressed as follows (note that in order to simplify the notation, the slot and RB index are omitted).

$$\mathbf{y}_{k,c_k}^{dl} = \underbrace{\mathbf{H}_{k,c_k}^{dl}\mathbf{W}_k\mathbf{x}_k}_{\text{Desired signal } ⑦} + \underbrace{\sum_{i\in K_{dl}(i\neq k)} \mathbf{H}_{k,c_i}^{dl}\mathbf{W}_i\mathbf{x}_i}_{\text{gNB-to-UE interference } ⑥} + \underbrace{\sum_{j\in K_{ul}(j\neq k)} \mathbf{i}_{k,j}}_{\text{UE-to-UE interference } ③④} + \mathbf{n}_k^{dl}, \quad (5)$$

where

- $\mathbf{H}_{k,c_i}^{dl}\mathbf{W}_i\mathbf{x}_i$ indicates the $M \times 1$ signal received by the k-th UE from the c_i-th cell. It consists of the channel matrix $\mathbf{H}_{k,c_i}^{dl} \in C^{M\times N}$ between the gNB and the UE,

the transmit precoder $\mathbf{W}_i \in C^{N \times L_{dl}}$ applied at the gNB in the DL RB (n), and the transmitted data symbol vector $\mathbf{x}_i$ of size $L_{dl} \times 1$, where L_{dl} refers to the transmission rank in DL, i.e. the number of simultaneous MIMO spatial layers. The channel $\mathbf{H}^{dl}_{k,c_i}$ is modeled according to the 3-dimensional (3D) UMa channel model, defined in [30], including transmit and receive antenna gain, distance-dependent path loss, shadowing, and fast-fading effects. $\mathbf{x}_i$ includes the gNB transmission power per RB for each layer which is denoted as $P^{RB}_{\text{Tx gNB}}$, while the total transmission power is controlled by conditioning $\|\mathbf{W}_i\|_F = 1$, where $\|.\|_F$ refers to the Frobenius norm.

- $\mathbf{i}_{k,j}$ is the cross-link interference matrix received by the k-th UE from aggressor UE j. The details about the modeling of this interference are described in the next subsection, and
- $\mathbf{n}^{dl}_k$ is the thermal noise at each receiver antenna represented as a $M \times 1$ vector whose entries are i.i.d. complex Gaussian distributed with zero mean and variance σ^2_n.

Similarly, the UL signal $\mathbf{y}^{ul\ (n,t)}_{k,c_k}$ received at the gNB c_k from the k-th UE at time instant t and over a specific resource block (n), is defined as:

$$\mathbf{y}^{ul}_{k,c_k} = \underbrace{\mathbf{H}^{ul}_{c_k,k}\mathbf{O}_k\mathbf{x}_k}_{\text{Desired signal } (8)} + \underbrace{\sum_{j \in K_{ul}(j \neq k)} \mathbf{H}^{ul}_{c_k,j}\mathbf{O}_j\mathbf{x}_j}_{\text{UE to gNB interference } (5)} + \underbrace{\mathbf{i}_{\text{SI}}}_{\text{gNB self-Interference } (1)} + \underbrace{\sum_{i \in \mathcal{C}(i \neq j)} \mathbf{i}_{c_k,c_j}}_{\text{gNB to gNB interference } (2)} + \mathbf{n}^{ul}_{c_k}, \quad (6)$$

where,

- $\mathbf{H}^{ul}_{c_k,k} \in C^{N \times M}$, $\mathbf{O}_k$, and $\mathbf{x}_k$ represent the channel matrix between transmitter and receiver, the $M \times L_{UL}$ UE transmit precoder matrix, and the $L_{UL} \times 1$ transmitted data symbols, respectively.
- $\mathbf{i}_{\text{SI}}$ refers to the interference from c_k gNB DL to its own UL.
- $\mathbf{i}_{c_k,c_j}$ is the interference generated from the gNB c_j towards gNB c_k.

The detailed modeling of $\mathbf{i}_{\text{SI}}$ and $\mathbf{i}_{c_k,c_j}$ are presented in the next subsections. We strive for presenting interference models that are broadly applicable to various scenarios and endorsed by a large number of partners in 3GPP.

1) Self-Interference Modeling

The gNB self-interference ($\mathbf{i}_{\text{SI}}$) refers to the interference generated from the gNB's DL transmission to its own UL reception. The large power difference between the received UL signal and the transmitted DL signal represents a major impairment to the UL reception. Extensive research has been carried out in the domain of self-interference cancellation for traditional full duplex, see e.g. [3], [11], [31]–[35]. In the context of SBFD, the following main techniques for self-interference mitigation have been identified in the ongoing Release 18 study in 3GPP [21]: i) frequency separation, ii) antenna isolation, iii) digital interference cancellation, and iv) beam-nulling techniques, as also summarized in Table 1. The combination of one or more of those defines the *ratio of self-interference* (RSI), which indicates the self-interference power in each UL RB relative to the gNB transmit power in each DL RB. The frequency separation aims to reduce the self-interference by separate DL and UL RBs (as compared to the traditional full duplex where DL and UL fully overlap) including the isolation effect of guard-band RBs. Antenna isolation refers to the use of separate transmit and receive antennas at the gNB (with potentially mechanical barriers to maximize the isolation [3]). According to [21], up to 45 dB and 80 dB of isolation can be achieved by these two methods, respectively. The 45 dB of frequency separation corresponds to the 3GPP requirement for the adjacent channel leakage ratio (ACLR), expressing the ratio of the transmitted power on the assigned channel, to the power received in the adjacent radio channel (e.g. assigned to another operator) [36]. Furthermore, the digital interference cancellation techniques can be employed to remove remaining interference in the digital base-band, by estimating the linear component from the received signal [37]. Beam-formed transmission can also be used to increase the RSI, providing that transmit antenna signals are transmitted in a null-space of the self-interference channel, which is nulled when arriving at the receive antennas [38]. Note that 0 dB is assumed as the minimum possible value for digital interference cancellation and beam nulling since the feasibility of these two techniques is still under discussion in 3GPP.

TABLE 1. Self-interference mitigation techniques values [39].

RSI component	Value [dB]
Frequency separation	45
Antenna isolation	[50 - 80]
Digital interference cancellation	[0 - 50]
Beam nulling	[0 - 40]
Overall RSI	[95 - 185]

The self-interference is represented as a vector $\mathbf{i}_{\text{RSI}} = [I_{\text{RSI},1}, ..., I_{\text{RSI},N}]^{\text{T}}$ (where $[.]^{\text{T}}$ refers to the transpose operation), whose elements indicate the signal received on each gNB receive antenna. The self-interference components are modeled as white Gaussian random variables [36]. The reason for such modeling is that this leakage interference is generated from non-linear effects on the transmitter side, especially at the power amplifier (PA) RF component. The exact signal distortion introduced by the PA is not fully known at the transmitter (nor at the receiver) and therefore it cannot be completely suppressed using digital pre-distortion techniques. For simplicity, it is consequently assumed that such components are raising the noise floor in each receiver antenna, i.e. $I_{\text{RSI},k} \sim \mathcal{N}(0, \sigma^2_{\text{RSI}})$, where the power of the self-interference equals the variance of the Gaussian distri-

bution σ^2_{RSI} which is calculated as:

$$\sigma^2_{\text{RSI}} = \frac{P^{RB}_{\text{Tx gNB}}}{\alpha_{\text{RSI}}} \times \frac{N_{\text{used-DL-RBs}}}{D_{RB}}\,, \tag{7}$$

where α_{RSI} refers to the RSI and $N_{\text{used-DL-RBs}}$ is the number of scheduled DL RBs at the current TTI. Essentially, the equation in (7) implies that the self-interference power equals $P^{RB}_{\text{Tx gNB}}/\alpha_{RSI}$ under full DL load conditions ($N_{\text{used-DL-RBs}} = D_{RB}$), while it reduces linearly under fractional DL load conditions (i.e. $N_{\text{used-DL-RBs}} < D_{RB}$). The RSI is the main parameter determining the impact of self-interference on UL RBs relative to the DL transmit power $P^{RB}_{\text{Tx gNB}}$. In dB domain, α_{RSI} can be expressed as the sum of one or more methods for self-interference mitigation (see Table 1) as follows:

$$\text{dB}(\alpha_{\text{RSI}}) \approx \text{dB}(\alpha_{\text{Tx-Rx isolation}}) + \text{dB}(\alpha_{\text{freq. separation}}) + \dots\,, \tag{8}$$

where dB() refers to the conversion from linear to dB, i.e. $\text{dB}(x) = 10\log_{10}(x)$. Note that (8) is used to exemplify the individual components contributing to achieving the RSI, although in practice the individual RSI components may have some dependencies. As an example, [3] shows that digital interference cancellation is only feasible under the condition of sufficient antenna isolation between the transmit and receive antennas. Under such conditions, 130 dB self-interference mitigation capability was achieved in the prototype in [20] as a combination of 55 dB antenna isolation, 45 dB ACLR and 30 dB sub-band filtering, and digital cancellation.

In each TTI t, the experienced self-interference $\mathbf{i}_{\text{RSI}}$ is assumed to be the same in any of the $1, ..., U_{\text{RB}}$ RBs in the UL sub-band, regardless of the separation of the UL RB with respect to RBs in the DL sub-band. This is regarded as a *frequency-flat* interference model, and is motivated by the typical spectral emission masks (SEM) of cellular base stations [40], [41]. In short, the assumption is that the gNB emissions are considerably high in the RBs immediately adjacent to the DL sub-band, while the emissions significantly reduce and become relatively constant upon a certain minimum frequency separation between the DL and UL RBs. By assuming a sufficiently large guard-band G_{RB} between DL and UL sub-band, to provide adequate isolation, the frequency-flat interference model becomes a reasonable assumption.

2) gNB-to-gNB Interference Modeling

DL transmissions on one cell interfere the UL reception of a neighbor cell during SBFD slots or symbols. For UMa scenario, gNB-to-gNB interference $\mathbf{i}_{c_k,c_j}$ can originate from cells c_k and c_j located in the same macro site (i.e. *intra-site* interference), or located on different sites (*inter-site* interference). Given the significantly distinct propagation characteristics, different modeling is proposed for these two cases as explained in the following.

In the case of intra-site gNB-to-gNB interference, the 3GPP 3D channel models [30] cannot be applied to estimate the spatial channel between cells on the same site. Therefore,

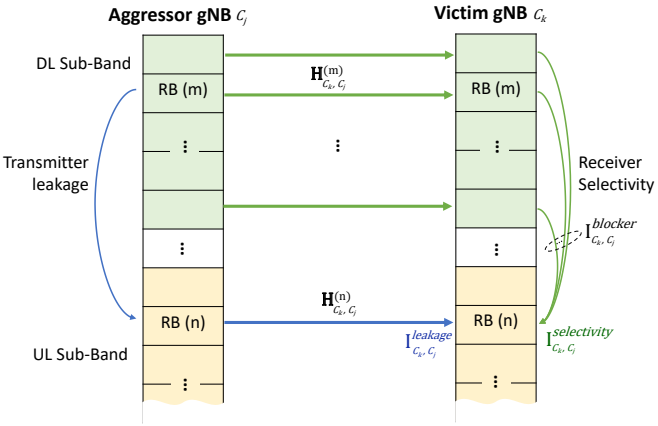

FIGURE 5. Transmitter leakage and receiver selectivity effects.

3GPP has agreed to use the same white noise-based modeling as for self-interference [36], where the interference power generated from one aggressor cell towards another cell deployed in the same site is defined as:

$$\sigma^2_{\text{gNB-intra-site}} = \frac{P^{RB}_{\text{Tx gNB}}}{\alpha_{\text{intra-site}}} \times \frac{N_{\text{used-DL-RBs}}}{D_{RB}}\,, \tag{9}$$

Comparing (7) and (9), the only difference is the use of $\alpha_{\text{intra-site}}$, which includes the effect of inter-sector isolation as well as frequency separation. Considering that cells in the same macro site are typically pointing in different directions, most of the interference will be received from the sidelobes and back lobes of the antenna. Therefore for simplicity, it is assumed a similar level of isolation as for self-interference, i.e. $\alpha_{\text{intra-site}} = \alpha_{\text{RSI}}$.

For the gNB-to-gNB inter-site interference $\mathbf{i}_{c_k,c_j}$, the impact of an aggressor cell c_j towards the victim cell c_k is twofold:

$$\mathbf{i}_{c_k,c_j} = \mathbf{i}^{\text{leakage}}_{c_k,c_j} + \mathbf{i}^{\text{selectivity}}_{c_k,c_j}\,. \tag{10}$$

As illustrated in Fig. 5, first, leakage emissions ($\mathbf{i}^{\text{leakage}}_{c_k,c_j}$) from the aggressor cell, due to the non-linear nature of the power amplifier, may increase the interference in the UL subband at the victim cell. Second, the non-ideal receiver frequency selectivity ($\mathbf{i}^{\text{selectivity}}_{c_k,c_j}$) in the victim cell, may result in leakage of the power received on the DL subband to the UL chains of the receiver.

The gNB-to-gNB leakage interference in the UL RB (n) is modeled as $\mathbf{i}^{\text{leakage}}_{c_k,c_j} = \mathbf{H}_{c_k,c_j}\mathbf{W}_{c_j}\mathbf{z}_{c_j}$, where $\mathbf{H}_{c_k,c_j}$ corresponds to the $N \times N$ channel matrix between cells c_k and c_j, and $\mathbf{W}_{c_j}$ refers to the transmit precoder of the aggressor gNB. Since the interference is coming from unwanted leakage emissions at the transmitter side, the equivalent $\mathbf{W}_{c_j}$ at the receiving band is modeled as a $N \times N$ identity matrix with the unitary norm, i.e. $\left\|\mathbf{W}_{c_j}\right\|_F = 1$. This is in line with the agreed assumptions in [36]. The vector $\mathbf{z}_{c_j} = [z_1, ..., z_N]^{\text{T}}$ provides the leakage signal at each transmit antenna of ag-

gressor cell c_j which is modeled as white Gaussian noise, e.g. $z_k \sim \mathcal{N}(0, \sigma^2_{\text{gNB-leakage}})$, with average power:

$$\sigma^2_{\text{gNB-leakage}} = \frac{P^{RB}_{\text{Tx gNB}}}{\alpha_{ACLR}} \times \frac{N_{\text{used-DL-RBs}}}{D_{RB}}\,, \tag{11}$$

where α_{ACLR} is the ACLR of the gNB transmitter, expressing the power that leaks in adjacent RBs relative to the transmit power in the DL subband.

For the receiver selectivity, the adjacent channel selectivity (ACS) determines the receiver's ability to operate under the presence of a strong interfering signal in the adjacent (DL) subband [23]. For the purposes of performance evaluation, the total interference power received over the DL subband caused by the DL transmission of cell c_j (also referred to as *blocker interference*) and averaged over the N receive antennas is first calculated as follows:

$$i^{\text{blocker}}_{c_k,c_j} = \frac{1}{N} \sum_{m \in \mathcal{D}} |\mathbf{H}^{(m)}_{c_k,c_j} \mathbf{W}^{(m)}_{c_j} \mathbf{s}^{(m)}_{c_j}|^2\,, \tag{12}$$

where $\mathcal{D} = \{1, ..., D_{RB}\}$ denotes the set of DL RBs in each cell, $\mathbf{H}^{(m)}_{c_k,c_j}$ represents the $N \times N$ channel between the cells, $\mathbf{W}^{(m)}_{c_j}$ the applied $N \times L_{dl}$ DL precoding matrix at the cell c_j and $\mathbf{s}^{(m)}_{c_j}$ the $L_{dl} \times 1$ DL symbols transmitted by cell c_j in the m-th DL RB of the aggressor gNB.

Based on the blocker interference in the DL subband, the interference present in the UL RB n due to selectivity is modeled as white Gaussian Noise, i.e. $\mathbf{i}^{\text{selectivity}}_{c_k,c_j} = [x_1, ..., x_N]^{\text{T}}$ where $x_k \sim N(0, \sigma^2_{\text{gNB-selectivity}})$ with average power $\sigma^2_{\text{gNB-selectivity}}$ determined as a ratio (defined by α_{ACS}) of the blocker interference:

$$\sigma^2_{\text{gNB-selectivity}} = \frac{\mathbf{i}^{\text{blocker}}_{c_k,c_j}}{\alpha_{ACS}}\,, \tag{13}$$

where α_{ACS} denotes the adjacent channel selectivity of the cell.

3) UE-to-UE Interference Modeling

UL leakage emissions from one UE's UL transmission generates interference to the DL reception of another UE during SBFD slots or symbols. The UE-to-UE leakage interference received by UE k ($k \in K_{dl}$) at the DL RB m, as a result of a simultaneous transmission at UE j ($j \in K_{ul}$) in an UL RB v is modeled as follows:

$$\mathbf{i}_{k,j} = \mathbf{H}_{k,j} \mathbf{O}_j \mathbf{z}_j, \tag{14}$$

where $\mathbf{H}_{k,j}$ corresponds to the $M \times M$ channel matrix between UEs k and j at the RB m, which includes the distance-dependent path-loss, slow and fast fading effects according to the 3D Urban Micro (UMi) channel model [30]. Since the scenario includes both outdoor and indoor UEs, the UMi model is extended according to [42] to include building penetration losses for indoor-to-outdoor UE links and indoor-to-indoor UE links placed in different buildings. These assumptions are in line with the agreements in 3GPP [36]. In (14), $\mathbf{O}_j$ refers to the UL transmit precoding at the aggressor UE in the UL RB m. Similar to the gNB-to-gNB CLI modeling, since the interference is generated from unwanted leakage emissions and there is no UL transmission from the aggressor UE on the RB of interest, $\mathbf{O}_j$ is modeled as an $M \times M$ identity matrix with the unitary norm. $\mathbf{z}_j$ is the M-dimensional column vector that models the leakage interference at each UE transmit antenna, with each component following a Gaussian distribution with an average power of:

$$\sigma^2_{\text{UE-leakage}} = \frac{P^{RB}_{\text{UE}\,j\,\text{Tx}}}{\alpha^{(m,v)}_{IBE_j}}\,, \tag{15}$$

where $P^{RB}_{\text{UE}\,j\,\text{Tx}}$ represents the transmit power per RB of the j-th UE (note that $P^{RB}_{\text{UE}\,j\,\text{Tx}}$ is time-varying and UE-dependent following the UL power control procedure in Section II-D), and $\alpha^{(m,v)}_{IBE_j}$ is the UE leakage power ratio from the RB v to the RB of interest m. Contrary to the *frequency-flat* leakage model assumed for the base station, the 3GPP specifications [41] provide a more detailed representation of the UE transmission leakage known as the in-band emission (IBE) model. In this IBE model, the power leakage is a function of the UE transmit power, selected MCS, and number of RBs in the allocation of the aggressor UE, as well as the frequency separation (i.e. number of RBs) between the UL allocation and DL allocation.

Fig. 6 shows an example of the UE spectral emission mask for a 10 RB allocation with 23 dBm transmission power (resulting in a transmit power per RB of 13 dBm). According to the 3GPP model, the UE emission is the sum of three components denoted as general, carrier leakage, and in-phase quadrature (IQ) image , where the carrier leakage is only present in the RB(s) in the middle of the carrier bandwidth, while the IQ image applies to the *mirrored* allocation on the opposite side of the carrier. Note that for the adopted SBFD frame structure where the UL RBs are placed in the middle of the carrier, both the IQ image and carrier leakage components are contained in the UL subband meaning that only the general component will have an impact on other UEs' DL reception (with $\sigma^2_{\text{UE-leakage}}$ between −12 dBm to −22 dBm as per the example in Fig. 6).

The detailed calculations of each IBE component are described in Table 2, where the error vector magnitude (EVM) denotes the limit specified for the modulation format used in the allocated RBs. Δ_{RB} indicates the starting frequency offset between the allocated RB and measured non-allocated RB (e.g. Δ_{RB} = 1 or Δ_{RB} = -1 for the first adjacent RB). Finally, P^{UE}_{RB} refers to the average of transmit power per RB measured in dBm.

IV. EVALUATION METHODOLOGY AND ASSUMPTIONS

The SBFD performance evaluation is conducted using advanced system-level simulations. The simulator is capable of modeling 3D multi-path channel models and realistic antenna patterns as specified by 3GPP [44]. It follows the latest 3GPP guidelines on SBFD evaluation methodology and it supports detailed modeling of 5G NR resource management

TABLE 2. IBE components description [43].

Component	Value
General [dB]	$\max\{-25 - 10\log_{10}(N_{\text{used-UL-RBs}}/U_{RB}),$ $20\log_{10}(\text{EVM}) - 3 - 5(\lvert\Delta_{RB}\rvert - 1)/U_{RB},$ $-57\text{dBm} + 10\log_{10}(\text{SCS}/15\text{kHz}) - P_{\text{Tx}}^{\text{UE}}\}$
IQ Image [dB]	-28 if $(P_{\text{Tx}}^{\text{UE}} > 10$ dBm), -25 if $(P_{\text{Tx}}^{\text{UE}} \leq 10$ dBm)
Carrier Leakage [dBc]	-28 if $(P_{\text{Tx}}^{\text{UE}} > 10$dBm), -25 if $(0$ dBm $\leq P_{\text{Tx}}^{\text{UE}} \leq 10$ dBm), -20 if $(-30$ dBm $\leq P_{\text{Tx}}^{\text{UE}} < 0$ dBm), -10 if $(-40$ dBm $\leq P_{\text{Tx}}^{\text{UE}} < -30$ dBm)

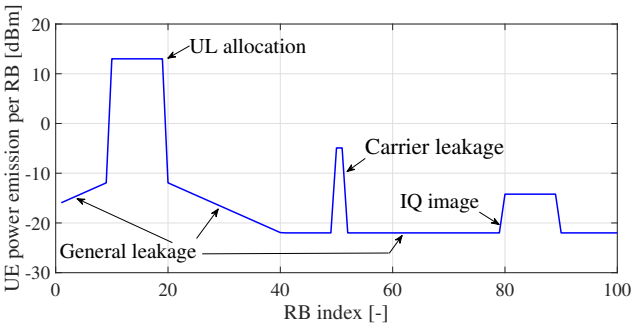

FIGURE 6. The UE IBE components.

mechanisms, such as link adaptation, dynamic scheduling, and power control, among others, and has been extensively calibrated against other companies' simulators [45].

The main simulation assumptions are summarized in Table 4. The network design and UE distribution follow the system model presented in Section II-A. The simulated scenario is a single-operator UMa deployment with $C = 21$ cells and $U = 210$ uniformly distributed static UEs. Each UE selects its candidate cell for connection based on the highest reference signal received power (RSRP). Each UE generates DL and UL traffic following the FTP3 model [46]. In short, the FTP3 mode produces data packets according to a homogeneous Poisson point process, where each packet is having a fixed size (assumed to equal 100 KBytes in this study). The average packet arrival rate is fine-tuned to generate three different load conditions, namely, low, medium, and high load. The average offered load of $L^{dl} = 43.2$ Mbps and $L^{ul} = 3.2$ Mbps at low load, $L^{dl} = 96$ Mbps and $L^{ul} = 12$ Mbps at medium load, and $L^{dl} = 212$ Mbps and $L^{ul} = 27.2$ Mbps at high load, are configured for each cell. These offered loads values result in an average RB load of 9%, 20%, and 55% in DL and 8%, 26%, and 52% in UL, which means the percentage of RBs allocated from the available RBs in each direction, for the TDD configuration which is used as the baseline for the purposes of comparison. Static TDD serves as the baseline for evaluating SBFD performance as this is the default duplexing scheme for current 5G deployments in unpaired bands. The deployed cells are assumed to be time-synchronized and to follow the same SBFD frame configuration, which resembles the configuration shown in Fig. 2. The SBFD frame configuration is designed to have a similar number of resource elements (REs) as TDD in each direction. Details of RB allocation and the corresponding number of REs for DL, UL, and guard-band in SBFD and DL, UL, and guard-period in TDD frame configurations are presented in Table 3, where γ_{RE} refers to the relative differences in the number of REs between the SBFD and TDD configurations.

TABLE 3. Details of SBFD frame configuration and TDD baseline.

Duplexing Scheme	Avalaible Resources
TDD	"DDDSU" D=DL slot, U=UL slot, S= 12 DL symbol + 2 guard symbol $D_{\text{RE}} = 176904$, $U_{\text{RE}} = 45864$, $G_{\text{RE}} = 6552$
SBFD	"XXXXX" X= DL+G+UL+G+DL $D_{\text{RB}} = 208$ RB, $U_{\text{RB}} = 55$ RB, $G_{\text{RB}} = 10$ RB $D_{\text{RE}} = 174720$, $U_{\text{RE}} = 46200$, $G_{\text{RE}} = 8400$
Ratio in % (SBFD/TDD - 1)	γ_{RE}^{DL}= -1.2 % γ_{RE}^{UL}= +0.7 %

For every transmission, SINR calculations are performed at OFDM-symbol-subcarrier resolution at the corresponding receiver end. All the sources of interference, including the SBFD-specific interference types, are accounted for during each SINR calculation in UL and DL direction according to (5) and (6), respectively. The calculated SINR over the bandwidth of interest is mapped to the mean mutual information per bit (MMIB) to form an effective SINR value [47]. This value is then mapped to BLEP which is dependent on the selected MCS. In cases of decoding errors, asynchronous HARQ with chase combining is used at both gNBs and UEs. The transmission of the HARQ feedback and retransmission(s) are modeled by taking into account the processing delay at both UE and gNB, as well as resource availability in both UL and DL. In DL, each UE explicitly acknowledges the corresponding gNB about the decoding outcome by transmitting HARQ feedback. In case of a decoding error, the gNB performs a HARQ re-transmission in the next available DL slot [48]. In UL, the gNBs do not explicitly indicate the decoding outcome, instead a retransmission grant is only transmitted if there is a need for a HARQ retransmission. The radio resource management schemes presented in Section II-D are also included in the simulations.

The conducted simulations are run for a sufficiently long time to ensure statistically reliable results, which allow us to draw solid conclusions. Monte Carlo methodology is applied to generate statistically independent snapshots of the simulated scenarios with randomized UE positions in each snapshot. The simulation time of each snapshot is adjusted to achieve at least 10 received packets per UE and a total of 10 snapshots are simulated to create a sufficient number of samples for the main KPI, presented in Section II-B. Afterwards, the results of each realization are jointly processed and results are presented in the next section. The empirical cumulative distribution function (CDF) of the users throughput is generated and different percentiles of the CDF are analyzed.

TABLE 4. Simulation assumptions

Parameter	Value
Network env.	3GPP Urban Macro (UMa) network with 21 cells, 500 meter inter-site distance and 25 meter gNB height
PHY settings	30 kHz subcarrier spacing; 12 subcarriers per RB; TTI size of 14 OFDM symbols
Carrier config.	100 MHz carrier bandwidth (273 RBs) at 4 GHz carrier frequency
Antenna configuration	gNB: $(M_g, N_g, P_g) = (8, 8, 2)$ with 32 transmit/receive chains. Directive radiation pattern with 8 dBi gain as in [49] UE: $(M_g, N_g, P_g) = (1, 2, 2)$ with 2 transmit and 4 receive chains and isotropic radiation pattern
MIMO	Dual-stream single-user MIMO with Type-I codebook-based precoder
Transmit Power	gNB max TX power: 53 dBm UE max TX power: 23 dBm
Receivers	gNB: LMMSE-IRC; 5 dB of noise figure UE: LMMSE-IRC; 9 dB of noise figure Thermal noise: -174 dBm/Hz
HARQ	Chase combining with max. HARQ retransmissions = 6
Link adaptation	BLER target = 10% with OLLA [25]
Power control	p_0 = -80 dBm; $\alpha = 0.7$
Radio propagation channel models	gNB to gNB: UMa with $h_{UE} = 25$ m and line of sight (LOS) probability of 0.75 to other base stations gNB to UE: UMa [30] UE to UE: Urban Micro (UMi)
UE distribution	210 uniformly distributed UEs. 80 % in indoor locations and 20 % outdoor [30]. Static UEs with fast fading speed of 3 km/h
Traffic model	Packet size $B = 100$ KByte Low load: (λ^{dl}=5.4) (λ^{ul}=0.4) Medium load: (λ^{dl}=12) (λ^{ul}=1.5) High load: (λ^{dl}=26.5) (λ^{ul}=3.4)
Packet scheduler	DL: Proportional fair with max. 6 scheduled UEs per TTI UL: Adaptive transmission bandwidth with max. 6 scheduled UEs per TTI
Interference modeling	$\alpha_{\text{RSI}} = [135, 149, 160]$ dB $\alpha_{\text{intra-site}} = [135, 149, 160]$ dB $\alpha_{\text{ACLR}} = 45$ dB $\alpha_{\text{ACS}} = 46$ dB

V. SBFD PERFORMANCE ANALYSIS

In this section, the effects of different interference components on the SBFD performance are evaluated by system-level simulations. Furthermore, the SBFD performance with diverse interference mitigation capabilities is studied and compared with TDD as the baseline. Different RSI values are assumed to resemble various self- and intra-site gNB-to-gNB interference mitigation capabilities. As a starting point, a 149 dB RSI is derived such that the noise floor of the gNB receiver is only increased by 1 dB as the consequence of self-interference. Additionally, other RSI values including 135 and 160 dB are simulated to show the performance of SBFD with conservative and advanced interference mitigation capabilities. How to achieve the different RSI values depends on the suppression capabilities as detailed in Table 1.

A. UL USER THROUGHPUT

Fig. 7 illustrates the 5%-ile UL user throughput for TDD and SBFD for different RSI values and offered load conditions. The green bar refers to ideal SBFD without any CLI, where only the legacy co-channel interference is present. At low load, the 5%-ile (corresponding to cell-edge users) experiences two times higher UL throughput in SBFD with 135 dB and four times with 149 dB or higher RSI, compared to TDD. At medium load, only SBFD with 149 dB or higher RSI values increases 5%-ile UL throughput, up to four times. Finally, at high load scenarios, even a very high RSI value is not able to improve the cell-edge UL throughput, except for the ideal SBFD case without any CLI. This shows that SBFD gains on 5%-ile UL throughput decrease by increasing the load due to a higher number of allocated DL RBs, which increases the severity of both self- and gNB-to-gNB interference. Higher RSI values can help to mitigate self- and intra-site interference at medium load while inter-site gNB-to-gNB is still damaging the SBFD performance.

The reason for this notable improvement of 5%-ile UL user throughput is the effect of UL resources being spread more in time for SBFD compared to TDD configuration, which allows users to transmit more often in the UL direction. According to the histogram of the number of allocated RBs per UE UL allocation shown in Fig. 8, for SBFD, the number of allocations with a small number of RBs ([1-5] RBs) is 4.6 times higher than TDD. Note that small RB allocations typically correspond to cell-edge users who can only transmit over the limited number of RBs before reaching their maximum transmit power (P_{max} in (4)). This means that cell-edge users have the opportunity to transmit in UL direction more frequently, while the number of UL allocations for cell-center UEs (with a large number of RBs, e.g.> 50) is similar for TDD and SBFD. Similarly, the CDF of the UE transmit power per UL allocation in Fig. 9 shows that 86% of the UL transmissions reach $P_{max} = 23$ dBm in TDD, whereas it is 65% in the case of SBFD. This indicates fewer UEs reach the maximum transmit power for UL transmission in SBFD due to an overall smaller RB allocation.

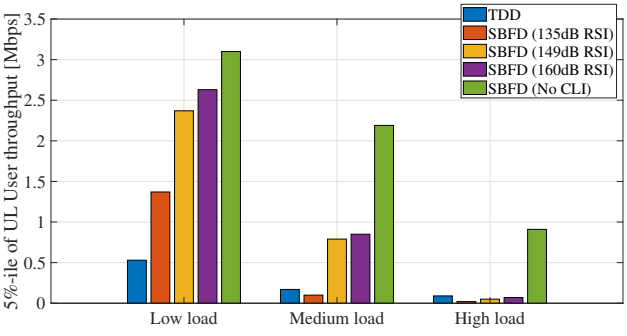

FIGURE 7. 5%-ile of users UL throughput in TDD compared to SBFD with different RSI values.

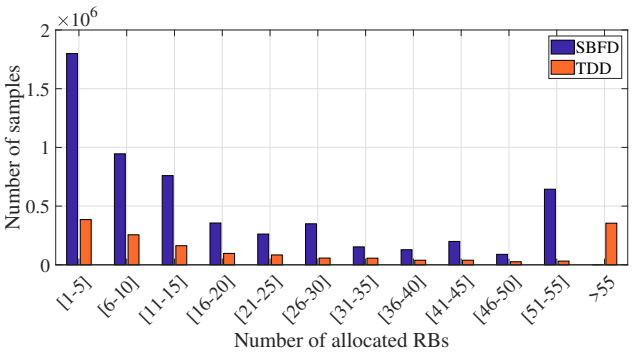

FIGURE 8. Histogram of the number of allocated RBs in each scheduled UL transport block during the simulation time for SBFD (RSI = 149 dB) and TDD at medium load.

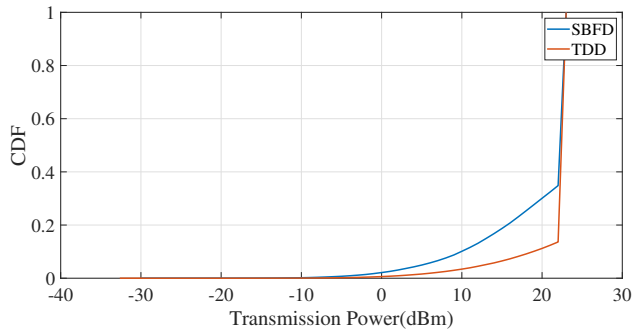

FIGURE 9. CDF of transmit power per transport block for SBFD (RSI = 149 dB) and TDD at medium load.

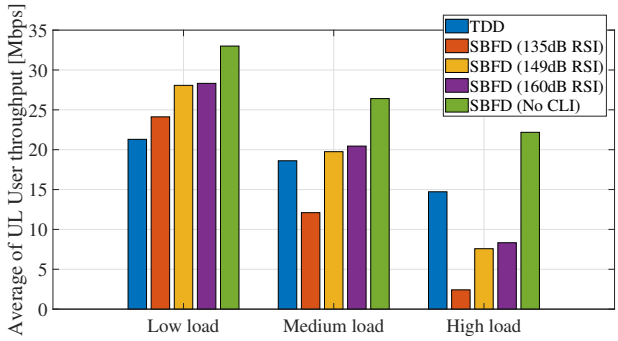

FIGURE 10. Average of users UL throughput for TDD and SBFD with varied RSI levels.

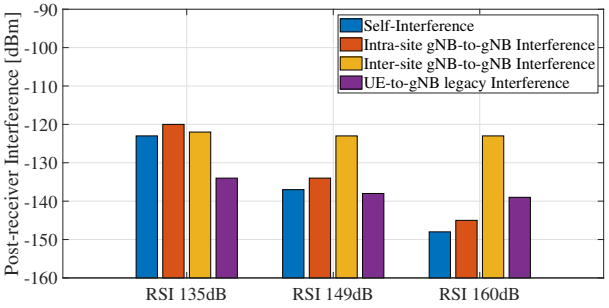

FIGURE 11. Average power of different interference components in UL direction for SBFD at medium load. The interference power is calculated as the average of the interference measurements in each (30 kHz) UL subcarrier.

In Fig. 10, the average UL user throughput is presented for TDD and SBFD. At low load, the average of the users UL throughput in SBFD is higher than TDD even with 135 dB RSI. At medium load, SBFD can provide a higher UL throughput than TDD with 149 dB or higher RSI values. Finally, at high load scenarios, only ideal SBFD without any CLI provides a higher UL throughput than TDD. As mentioned before, the inter-site gNB-to-gNB interference increases with a higher offered load (more allocated DL RBs), and highly damages the users UL throughput in SBFD at high load.

To understand the effects of the SBFD interference on the UL throughput performance, Fig. 11 shows the average power of different interference types in UL direction at medium load for SBFD. As expected, in case of low RSI value of 135 dB, self-interference and gNB-to-gNB including both intra-site and inter-site interference damage the SBFD performance more or less in an equal manner. For higher RSI, the inter-site gNB-to-gNB becomes the main damaging factor with the highest interference power. In the case of 160 RSI the self- and intra-site interference power becomes even lower than legacy UE-to-gNB interference. This indicates that even with sufficient self- and intra-site interference mitigation, the inter-site gNB-to-gNB interference is limiting the SBFD gain on the UL throughput.

B. DL USER THROUGHPUT

Fig. 12 and 13 show the average and CDF of the DL user throughput for SBFD compared to TDD, respectively. The reason for the differences in users DL throughput for SBFD and TDD is that TDD configuration allows the packets to be fully transmitted in a shorter time than SBFD due to the larger availability of DL resources in DL slots. On the other hand, the difference between ideal SBFD and SBFD with CLI indicates the UE-to-UE interference (15) impact on DL transmission. Since the UEs are assumed to be uniformly distributed in the Urban Macro network, UEs are generally far away from each other and the UE-to-UE interference is not significant. Nevertheless, the UE-to-UE interference increases with the offered load due to the larger probability of having a UL UE transmitting while another UE is being served in the DL direction.

When analyzing the impact of different interference types on UL and DL throughput in a UMa environment, it is evident that gNB self-interference and gNB-to-gNB interference are the dominant effects on the SBFD performance, while the UE-to-UE and legacy interference only have minor effects. Nevertheless, after ensuring sufficient RSI, inter-site gNB-to-gNB interference emerges as the primary challenge in SBFD deployment.

To wrap up, Fig. 14 illustrates the relative gains of SBFD with 149 dB RSI in UL and DL user throughput compared to TDD baseline at different load conditions. At low load,

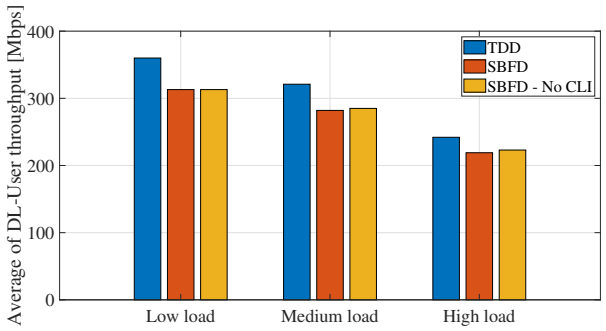

FIGURE 12. Average of the DL user throughput for TDD and SBFD with 149 dB RSI.

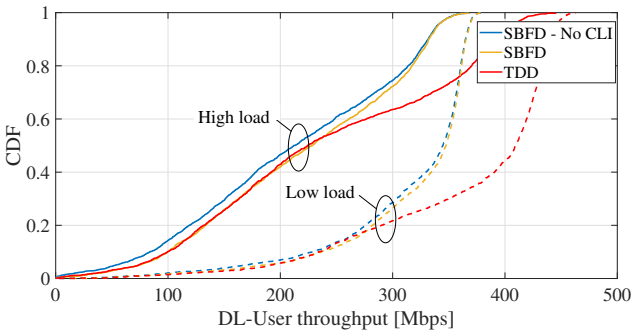

FIGURE 13. CDF of the DL user throughput for TDD and SBFD with 149 dB RSI.

SBFD provides 310% increase of cell-edge and 32% increase of average UL user throughput, while it causes a decrease of cell-edge and average DL user throughput by 4% and 13%, respectively. This goes to a 365% increase of cell-edge and 6% increase of average UL user throughput at medium load, with 7% and 12% decrease of 5%-ile and average DL user throughput, respectively. However, there is no positive gain in high load due to the inter-site gNB-to-gNB interference effect on SBFD performance: As the DL offered load increases, more DL RBs are allocated, which results in higher interference to the UL transmission and subsequently reduces the UL throughput. This means, the proposed SBFD configuration has the potential to significantly improve the UL throughput for cell-edge users as well as average UL user throughput with a minor decrease in DL throughput; but, this requires managing inter-site gNB-to-gNB interference in addition to sufficient self- and intra-site gNB-to-gNB interference mitigation. In DL, the lower average UE throughput for SBFD is a consequence of the lower availability of DL resources in 'X' slots as compared to TDD DL slots, which increases the time it takes to deliver the DL packets to the UE. Also, at high load, the SBFD cell-edge DL throughput reduces as much as 14% (compared to only 4% at low load) which can be attributed to the higher UE-to-UE interference due to higher UL load.

Finally, the required level of RSI is assessed in detail in Fig. 15, which shows the relative gains of SBFD at

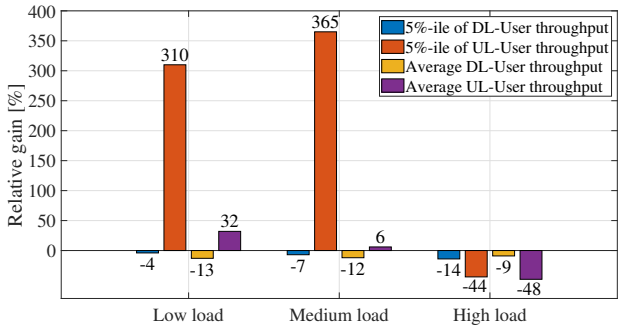

FIGURE 14. Relative gains in UL and DL user throughput for SBFD with 149 dB RSI compared to TDD.

medium load for six different RSI values. At medium load, the SBFD gain on 5%-ile users UL throughput is positive for 140 dB or higher RSI values while it is negative for lower RSI. The increase of 5%-ile UL user throughput becomes more significant with increasing the RSI value in addition to some increase in the average of the UL user throughput. However, more than 149 dB RSI does not result in significant improvement of the SBFD performance. This indicates that 149 dB RSI can be considered an appropriate value to have acceptable performance benefits of SBFD compared to TDD. This RSI value can be achieved by applying the interference techniques presented in Table 1. For instance, using a combination of 45 dB frequency separation and 80 dB antenna isolation, while the remaining 24 dB requires additional techniques such as digital interference cancellation and/or beam nulling which are still under study in 3GPP.

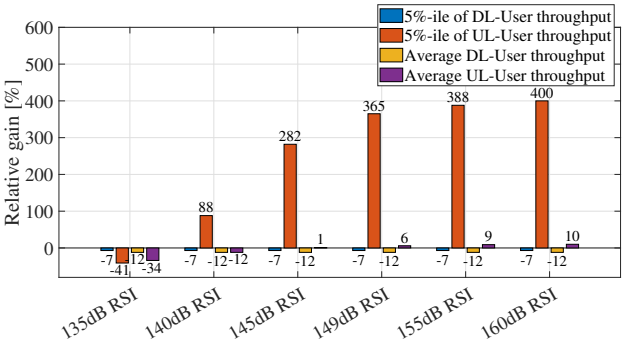

FIGURE 15. Relative gains in UL and DL user throughput for SBFD at medium load with different RSI values dB RSI compared to TDD.

The set of system-level performance results for SBFD cases that come closest to our results are those reported in [20]. There are, however, several differences in simulations assumption and modeling, that prevents a detailed one-to-one comparison of the results. Most notably, the results in [20] are for dense urban cases with 200 meters ISD and 40 dBm gNB transmit power (we assume 500 meters ISD and 53 dBm gNB transmit power), and a generalized memory polynomial (GMP) model for the self- and gNB-to-gNB interference modeling is assumed. Furthermore, [20] assumes two Tx/Rx antennas at the gNB, while we assume 32 antenna ports and

SU-MIMO with MMSE-IRC receivers. Taking these differences into account, we find a need for a higher RSI of 149 dB as compared to those in [20] due to differences in gNB transmit power and interference modeling. Secondly, as our simulated environment is more coverage limited with higher UE transmit power (due to the larger ISD), and assuming frame structure of XXXXX (while [20] assume XXXXU, i.e., more UL resources and less DL resources), our reported UL gain values are few percentage points lower, but with a smaller loss in the DL.

VI. CONCLUSION

In this work, SBFD is proposed as a novel duplexing method to improve UL throughput, by providing simultaneous UL and DL allocation on non-overlapping frequency resources. The precise modeling of different interference types is presented and used in highly detailed system-level simulations. For an Urban Macro scenario, simulation results indicate that SBFD with 149 dB ratio of self-interference (RSI) is able to increase the cell-edge UL throughput four times compared to static TDD as well as 32% and 6% increase of average UL user throughput at low and medium load, respectively. Lower RSI values (135-140 dB) provide a cell-edge UL throughput increase of only two times at low load, while no gains as compared to static TDD are observed at medium or high load. RSI values above 149 dB do not increase the SBFD gains significantly, since the inter-site gNB-to-gNB interference becomes the bottleneck in terms of UL performance. The UL throughput improvements come at a small cost of only 12% average UE DL throughput reduction.

Note that the SBFD results assumed the use of a separate transmit and receive antenna panel in the gNB which doubles the total number of antenna elements in order to keep the same antenna array gain as in TDD. This increase in gNB hardware size in addition to the higher gNB complexity due to the need for sophisticated interference mitigation techniques needs to be accounted for when determining the pros and cons of SBFD. Similarly, for future work, the feasibility and techniques for achieving 149 dB of RSI need to be further studied.

Future research directions include performance evaluation of SBFD also for other environment types such as low power gNB deployments, and performance comparison of SBFD versus traditional FD. Finally, studying coordinated beamforming (precoding techniques) as a potential method to further combat the gNB-to-gNB CLI is recommended to unleash the full performance gain of SBFD.

Acronyms

3GPP	Third Generation Partnership Project
5G	Fifth Generation of cellular networks
ACK	Acknowledgement
ACLR	Adjacent Channel Leakage Ratio
ACS	Adjacent Channel Selectivity
BLER	Block Error Rate
CDF	Cumulative Distribution Function
CLI	Cross Link Interference
CQI	Channel Quality Indicator
CSI	Channel State Information
DL	Downlink
EVM	Error Vector Magnitude
FD	Full Duplex
FDD	Frequency Division Duplexing
FTP3	File Transfer Protocol Model 3
GMP	Generalized Memory Polynomial
gNB	5G base station
HARQ	Hybrid Automatic Repeat reQuest
IQ	In-phase Quadrature
ISD	Inter-Site Distance
KPI	Key Performance Indicator
LOS	Line Of Sight
MCS	Modulation and Coding Scheme
MIMO	Multiple Input Multiple Output
MMIB	Mean Mutual Information per Bit
NACK	Negative Acknowledgement
NR	New Radio
OFDMA	Orthogonal Frequency-Division Multiple Access
OLLA	Outer Loop Link Adaptation
PA	Power Amplifier
PF	Proportional Fair
RB	Resource Block
RE	Resource Element
RRM	Radio Resource Management
RSI	Ratio of Self-Interference
RSRP	Reference Signal Received Power
SBFD	Sub-Band Full Duplex
SCS	Sub-Carrier Spacing
SEM	Spectral Emission Mask
SIC	Self-Interference Cancellation
SINR	Signal to Interference and Noise Ratio
SRS	Sounding Reference Signal
SU-MIMO	Single-User Multiple-Input Multiple-Output
TDD	Time Division Duplexing
TTI	Transmission Time Interval
UE	User Equipment
UL	Uplink
UMa	Urban Macro
UMi	Urban Micro
XDD	Cross Division Duplexing

REFERENCES

[1] W. Chen, J. Montojo, J. Lee, M. Shafi, and Y. Kim, "The standardization of 5G-advanced in 3GPP," IEEE Communications Magazine, vol. 60, no. 11, pp. 98–104, Jun. 2022.

[2] Y. Shi, E. Alsusa, and M. W. Baidas, "A survey on downlink-uplink decoupled access: Advances, challenges, and open problems," Computer Networks, p. 109040, Aug. 2022.

[3] H. Ji, Y. Kim, K. Muhammad, C. Tarver, M. Tonnemacher, T. Kim, J. Oh, B. Yu, G. Xu, and J. Lee, "Extending 5G TDD coverage with XDD: Cross division duplex," IEEE Access, vol. 9, pp. 51 380–51 392, Mar. 2021.

[4] K. Ardah, G. Fodor, Y. C. Silva, W. C. Freitas, and F. R. Cavalcanti, "A novel cell reconfiguration technique for dynamic TDD wireless networks," IEEE Wireless Communications Letters, vol. 7, no. 3, pp. 320–323, Nov. 2017.

[5] A. A. Esswie, K. I. Pedersen, and P. E. Mogensen, "Online radio pattern optimization based on dual reinforcement-learning approach for 5G URLLC networks," IEEE Access, vol. 8, pp. 132 922–132 936, Jul. 2020.

[6] H. Kim, J. Kim, and D. Hong, "Dynamic TDD systems for 5G and beyond: A survey of cross-link interference mitigation," IEEE Communications Surveys & Tutorials, vol. 22, no. 4, pp. 2315–2348, Jul. 2020.

[7] K. Pedersen, A. Esswie, D. Lei, J. Harrebek, Y. Yuk, S. Selvaganapathy, and H. Helmers, "Advancements in 5G new radio TDD cross link interference mitigation," IEEE Wireless Communications, vol. 28, no. 4, pp. 106–112, Apr. 2021.

[8] 3GPP TR 38.828, V16.0.0, "Cross link interference handling and remote interference management (RIM) for NR (Release 16)," Tech. Rep., Jun. 2019.

[9] X. Lin, "An overview of 5G advanced evolution in 3GPP release 18," IEEE Communications Standards Magazine, vol. 6, no. 3, pp. 77–83, Sep. 2022.

[10] K. I. Pedersen, G. Berardinelli, F. Frederiksen, and P. Mogensen, "A flexible 5G wide area solution for TDD with asymmetric link operation," IEEE Wireless Communications, vol. 24, no. 2, pp. 122–128, Nov. 2016.

[11] M. Duarte, C. Dick, and A. Sabharwal, "Experiment-driven characterization of full-duplex wireless systems," IEEE Transactions on Wireless Communications, vol. 11, no. 12, pp. 4296–4307, Nov. 2012.

[12] R. Askar, J. Chung, Z. Guo, H. Ko, W. Keusgen, and T. Haustein, "Interference handling challenges toward full duplex evolution in 5G and beyond cellular networks," IEEE Wireless Communications, vol. 28, no. 1, pp. 51–59, Feb. 2021.

[13] K. E. Kolodziej, In-Band Full-Duplex Wireless Systems Handbook. Artech House, 2021.

[14] H. Alves, T. Riihonen, and H. A. Suraweera, Full-Duplex Communications for Future Wireless Networks. Springer, 2020.

[15] K. E. Kolodziej, B. T. Perry, and J. S. Herd, "In-band full-duplex technology: Techniques and systems survey," IEEE Transactions on Microwave Theory and Techniques, vol. 67, no. 7, pp. 3025–3041, Feb. 2019.

[16] M. G. Sarret, G. Berardinelli, N. H. Mahmood, and P. Mogensen, "Impact of transport control protocol on full duplex performance in 5G networks," in 2016 IEEE 83rd Vehicular Technology Conference (VTC Spring). IEEE, Jul. 2016, pp. 1–5.

[17] M. G. Sarret, M. Fleischer, G. Berardinelli, N. H. Mahmood, P. Mogensen, and H. Heinz, "On the potential of full duplex performance in 5G ultra-dense small cell networks," in 2016 24th European Signal Processing Conference (EUSIPCO). IEEE, Dec. 2016, pp. 764–768.

[18] N. H. Mahmood, M. G. Sarret, G. Berardinelli, and P. Mogensen, "Full duplex communications in 5G small cells," in 2017 13th International Wireless Communications and Mobile Computing Conference (IWCMC). IEEE, Jul. 2017, pp. 1665–1670.

[19] V. Singh, A. Gadre, and S. Kumar, "Full duplex radios: Are we there yet?" in Proceedings of the 19th ACM Workshop on Hot Topics in Networks, Nov. 2020, pp. 117–124.

[20] X. Han, R. Liu, X. Liu, C. Liang, X. Wei, Y. Hao, Z. Zhang, and S. Jin, "Interference mitigation for non-overlapping sub-band full duplex for 5G-Advanced wireless networks," IEEE Access, vol. 10, pp. 134 512–134 524, Dec. 2022.

[21] 3GPP RP-213591, "Study on evolution of NR duplex operation (Release 18)," Tech. Rep., Dec. 2022.

[22] M. Enescu, 5G New Radio: A beam-based air interface. John Wiley & Sons, 2020.

[23] 3GPP R1-2211678, "Summary on evaluation on NR duplex evolution," Tech. Doc., Nov. 2022.

[24] M. Lampinen, F. Del Carpio, T. Kuosmanen, T. Koivisto, and M. Enescu, "System-level modeling and evaluation of interference suppression receivers in lte system," in 2012 IEEE 75th Vehicular Technology Conference (VTC Spring). IEEE, 2012, pp. 1–5.

[25] G. Pocovi, K. I. Pedersen, and P. Mogensen, "Joint link adaptation and scheduling for 5G ultra-reliable low-latency communications," IEEE Access, vol. 6, pp. 28 912–28 922, May 2018.

[26] C. Rosa, D. L. Villa, C. U. Castellanos, F. D. Calabrese, P.-H. Michaelsen, K. I. Pedersen, and P. Skov, "Performance of fast AMC in E-UTRAN uplink," in 2008 IEEE International Conference on Communications. IEEE, May 2008, pp. 4973–4977.

[27] 3GPP TS 38.213 V17.5.0, " NR; Physical layer procedures for control (Release 17)," Tech. Spec., Mar, 2023.

[28] A. Karimi and K. I. Pedersen, "5G system-level performance analysis of uplink multi-panel transmission in mm-wave frequencies," in 2021 IEEE 94th Vehicular Technology Conference (VTC2021-Fall). IEEE, Dec. 2021, pp. 01–06.

[29] F. D. Calabrese, C. Rosa, M. Anas, P.-H. Michaelsen, K. I. Pedersen, and P. E. Mogensen, "Adaptive transmission bandwidth based packet scheduling for lte uplink," in 2008 IEEE 68th Vehicular Technology Conference. IEEE, Sep. 2008, pp. 1–5.

[30] 3GPP TR 38.901, "Study on channel model for frequencies from 0.5 to 100 GHz (Release 14)," Tech. Rep., Mar. 2017.

[31] G. Liu, F. R. Yu, H. Ji, V. C. Leung, and X. Li, "In-band full-duplex relaying: A survey, research issues and challenges," IEEE Communications Surveys & Tutorials, vol. 17, no. 2, pp. 500–524, Jan. 2015.

[32] S. Li and R. D. Murch, "An investigation into baseband techniques for single-channel full-duplex wireless communication systems," IEEE Transactions on Wireless Communications, vol. 13, no. 9, pp. 4794–4806, Jul. 2014.

[33] S. Barghi, A. Khojastepour, K. Sundaresan, and S. Rangarajan, "Characterizing the throughput gain of single cell MIMO wireless systems with full duplex radios," in 2012 10th international symposium on modeling and optimization in Mobile, Ad Hoc and Wireless Networks (WiOpt). IEEE, Aug. 2012, pp. 68–74.

[34] C. D. Nwankwo, L. Zhang, A. Quddus, M. A. Imran, and R. Tafazolli, "A survey of self-interference management techniques for single frequency full duplex systems," IEEE Access, vol. 6, pp. 30 242–30 268, Nov. 2017.

[35] T. Kim, K. Min, and S. Park, "Self-Interference Channel Training for Full-Duplex Massive MIMO Systems," Sensors, vol. 21, no. 9, p. 3250, May 2021.

[36] 3GPP TR 38.858, "Study on evolution of NR duplex operation (Release 18)," Tech. Rep., May. 2023.

[37] V. Panse, T. K. Jain, P. K. Sharma, and A. Kothari, "Digital self-interference cancellation in the era of machine learning: A comprehensive review," Physical Communication, vol. 50, p. 101526, Feb. 2022.

[38] X. Huang, A. T. Le, and Y. J. Guo, "Transmit beamforming for communication and self-interference cancellation in full duplex MIMO systems: A trade-off analysis," IEEE Transactions on Wireless Communications, vol. 20, no. 6, pp. 3760–3769, Jan. 2021.

[39] 3GPP R4-2214376, "Reply LS on interference modelling for duplex evolution (Release 18)," Tech. Rep., Aug. 2022.

[40] T. Chapman, E. Larsson, P. von Wrycza, E. Dahlman, S. Parkvall, and J. Sköld, "Chapter 16 - spectrum and rf characteristics," in HSPA Evolution. Oxford: Academic Press, 2015, pp. 417–450.

[41] 3GPP TS 38.101-1 V18.0.0, "User Equipment Radio Transmission and Reception," Tech. Rep., Dec. 2022.

[42] 3GPP TR 38.802, " Study on new radio access technology Physical layer aspects (Release 114)," Tech. Rep., Sep. 2017.

[43] A. Kord and J. B. Coder, "On the impacts of in-band LTE emissions," in 2018 United States National Committee of URSI National Radio Science Meeting (USNC-URSI NRSM). IEEE, Feb. 2018, pp. 1–2.

[44] 3GPP TR 38.901, "Study on channel model for frequencies from 0.5 to 100 GHz (Release 17)," Tech. Rep., Mar. 2022.

[45] 3GPP TSG RAN WG1, "Summary on SLS calibration results for NR duplex evolution," Tech. Rep., Feb. 2023.

[46] 3GPP TR 36.814, "Evolved Universal Terrestrial Radio Access (E-UTRA); Further advancements for E-UTRA physical layer aspects (V9.2.0)," Tech. Rep., Mar. 2017.

[47] IEEE 802.16 Broadband Wireless Access Working Group and others, "IEEE 802.16 m evaluation methodology document (EMD)," IEEE 802.16 m-08/004r5, 2009.

[48] 3GPP 38.214 V17.4.0, "NR Physical layer procedures for data Technical Specification," Tech. Rep., Dec. 2022.

[49] M. Series, "Guidelines for evaluation of radio interface technologies for IMT-2020," Report ITU, vol. 2512, 2017.

MASOUMEH MOKHTARI (Student Member, IEEE) attained her M.Sc. degree in Information Technology engineering from the University of Isfahan, Iran, in 2019. Currently, she is a Ph.D. Fellow researcher at Aalborg University, Denmark. Her research interests include duplexing and radio resource management for cellular networks.

GUILLERMO POCOVI received his M.Sc. degree in telecommunications engineering from Universitat Politècnica de Catalunya in 2014, and his PhD from Aalborg University, Denmark, in 2017. He is currently with Nokia Standards, Aalborg. His research activities are related to the study and standardization of advanced duplexing techniques for 5G-Advanced.

ROBERTO MALDONADO received the M.Sc. degree in telecommunication engineering from University of Granada, Spain, in 2016 and the Ph.D. degree from Aalborg University, Denmark, in 2021. He is currently a Research Specialist with Nokia Standard. His research interests include flexible duplexing evolution and radio resource management enhancements for 5G and 5G-Advanced networks.

KLAUS I. PEDERSEN (Senior Member, IEEE) received an M.Sc. degree in electrical engineering and a Ph.D. degree from Aalborg University, Aalborg, Denmark, in 1996 and 2000, respectively. He is a Bell Labs Fellow at Nokia, currently leading the Radio Access Network Research Team in Aalborg, and a part-time External Professor at Aalborg University. He has authored publications on a wide range of topics, as well as an inventor on several patents. His current research interests include access protocols and radio resource management enhancements for 5G, 5G-Advanced, and 6G.